

On the narrow spectral feature at ~ 3 TeV in the MAGIC spectrum of Mrk 501

Wen Hu¹ and Dahai Yan^{2*}

¹*Department of Physics, Jingtangshan University, Jiangxi Province, Ji'an 343009, People's Republic of China*

²*Key Laboratory for the Structure and Evolution of Celestial Objects, Yunnan Observatories, Chinese Academy of Sciences, Kunming 650011, People's Republic of China*

Accepted XXX. Received YYY; in original form ZZZ

ABSTRACT

Using a time-dependent one-zone leptonic model that incorporates both shock acceleration and stochastic acceleration processes, we investigate the formation of the narrow spectral feature at ~ 3 TeV of Mrk 501 which was observed during the X-ray and TeV flaring activity in July 2014. It is found that the broadband spectral energy distribution (SED) can be well interpreted as the synchrotron and synchrotron-self-Compton emission from the electron energy distribution (EED) that is composed by a power-law (PL) branch and a pileup branch. The PL branch produces synchrotron photons which are scattered by the electrons of the pileup branch via inverse-Compton scattering and form the narrow spectral feature observed at the TeV energies. The EED is produced by two injection episodes, and the pileup branch in EED is caused by shock acceleration rather than stochastic acceleration.

Key words: acceleration of particles – radiation mechanisms: non-thermal – BL Lacertae objects: individual: Mrk 501

1 INTRODUCTION

The broadband spectral energy distributions (SEDs) of blazars can be characterized by a double-peak structure extending from radio frequencies to the γ -ray energies (Abdo et al. 2010a; Giommi et al. 2012; Acciari et al. 2021b). The low-energy peak located in the infrared to X-ray range is interpreted as synchrotron emission from non-thermal relativistic electrons accelerated in jets. Based on the position of the synchrotron peak (ν_{pk}), blazars are divided into high-synchrotron-peaked (HSP; $\nu_{\text{pk}} > 10^{15}$ Hz), intermediate-synchrotron-peaked (ISP; $10^{14} < \nu_{\text{pk}} < 10^{15}$ Hz), and low-synchrotron-peaked (LSP; $\nu_{\text{pk}} < 10^{14}$ Hz) blazars (Abdo et al. 2010b). The high-energy peak, located at γ -ray energies, can be well explained by leptonic models. γ -ray photons from HSPs are usually generated via inverse-Compton (IC) scattering the synchrotron photons by the same electron population that produces the synchrotron emission (SSC) (Maraschi, Ghisellini & Celotti 1992; Yan, Zeng & Zhang 2014).

Blazars exhibit fast and large-amplitude variability across the entire electromagnetic spectrum (e.g., Hayashida et al. 2012; Paliya, Sahayanathan & Stalin 2015; Bartoli et al. 2016; Yan et al. 2018). However, the physical origin of the variability and the associated electron acceleration mechanism are currently not well understood. Diffusive shock acceleration (e.g., Drury 1983; Kirk, Rieger & Mastichiadis 1998; Summerlin & Baring

2012) and stochastic acceleration (e.g., Dermer, Miller & Li 1996; Katarzyński et al. 2006; Yan, Zeng & Zhang 2012) are widely considered in blazar jets.

Mrk 501 is a famous TeV HSP (Quinn et al. 1996), which is intensively monitored by various astronomical detectors, from radio frequencies to TeV γ rays (e.g., Abdo et al. 2011; Neronov, Semikoz & Taylor 2012; Shukla et al. 2015; Aleksić et al. 2015; Ahnen et al. 2018). Very recently, an extreme X-ray activity in July 2014 was reported by Acciari et al. (2020). During the flaring activity, the X-ray and TeV emissions have been found to be correlated, and the amplitude of the TeV variability is twice as large as that of the X-ray variability. This indicates that the leptonic model is most likely favored. Interestingly, a narrow feature at ~ 3 TeV was observed by MAGIC stereoscopic telescope on 2014 July 19 (MJD 56857.98), and the significance of this peak-feature is estimated to be $\sim 4\sigma$ (Acciari et al. 2020). This kind of spectral feature is rare, which will provide insight into the underlying emission mechanism in the jet. Acciari et al. (2020) proposed several explanations for this narrow spectral feature, including pileup in the electron energy distribution due to stochastic acceleration and IC pair cascade induced by electrons accelerated in a magnetospheric vacuum gap. Wendel et al. (2021) provided details for IC pair cascade scenario.

Interestingly, Acciari et al. (2021a) reported that the X-ray flux measured by *Swift*-BAT in the 15–50 keV band is significantly higher than that expected from the simple extrapolation of the *Swift*-XRT spectral data for HSP Mrk 421 during MJD 57422–57429 (2016 February 4–11). This suggests an additional emission

* E-mail: yandahai@ynao.ac.cn

component beyond the single synchrotron emission (Acciari et al. 2021a). This BAT excess may be related to the presence of the additional (and narrow) component in the TeV spectrum of Mrk 501 (Acciari et al. 2021a). Actually, the results of *NuSTAR* data analysis have revealed possible excess in hard X-ray emission for Mrk 421 (Kataoka & Stawarz 2016) and PKS 2155-304 (Madejski et al. 2016). These results may imply that the appearance of the occasional TeV narrow spectral feature is not unique in Mrk 501. The future improved TeV γ -ray detectors, such as Cherenkov Telescope Array (CTA; e.g., Actis et al. 2011; Acharya et al. 2013; Sol et al. 2013), would detect such a narrow sharp feature with high significance.

Our goal is to interpret the narrow feature at ~ 3 TeV of Mrk 501 during the extreme X-ray activity in 2014 July 19 in the framework of a one-zone leptonic model. This paper is structured as follows: we describe our model in Section 2 and results in Section 3, followed by the discussion and conclusions in Section 4.

2 MODEL

Our model assumes a single, homogenous emission region of radial size R' , which moves along the jet with bulk Lorentz factor Γ . This region is assumed to be filled with random magnetic field with the strength of B' . The accelerated electrons in the region will radiate photons through synchrotron and inverse-Compton (IC) scattering processes. For an observer located at a small viewing angle θ_{obs} with respect to the jet, the radiative luminosity in the comoving frame is boosted by a factor of δ_{D}^4 , and the variability timescale is reduced by a factor of δ_{D}^{-1} (e.g., Urry & Padovani 1995). Here δ_{D} is the Doppler factor, which is given by $\delta_{\text{D}} = 2\Gamma/(1 + N_{\Gamma}^2)$, where $N_{\Gamma} \equiv \Gamma\theta_{\text{obs}}$ (Dermer et al. 2014). The emitting region size is constrained by the causality condition: $R' \lesssim ct_{\text{var}}\delta_{\text{D}}/(1+z)$, where t_{var} is the measured variability timescale and z is the blazar redshift. It is usually assumed $N_{\Gamma} = 1$, so that $\delta_{\text{D}} = \Gamma$ (e.g., Nalewajko, Begelman & Sikora 2014).

In the model, we take into account the synchrotron self-absorption, as well as the absorption for γ -ray photons caused by the interaction with the internal synchrotron radiation field. The numerical method to calculate such emission spectra is the same as that in Dermer & Menon (2009). Throughout the paper, quantities in the comoving frame of the emission region are primed, and those in the stationary frame or observer's frame are unprimed.

In the model, we do not distinguish the acceleration region from the emission region, and we assume that the distribution of relativistic emitting electrons is the result of the evolution of the injected electrons undergoing acceleration, energy losses and escape. To reduce the number of model parameters, the injection of electrons is assumed to be mono-energetic, which is given by the δ -function

$$\dot{Q}_{e,i}(\gamma', t') = \frac{L'_{\text{inj},i} \delta(\gamma' - \gamma'_{\text{inj},i})}{V' \gamma'_{\text{inj},i} m_e c^2} H(t'; T'_{s,i}, T'_{f,i}), \quad (1)$$

where $V' = 4\pi R'^3/3$ is the comoving volume of the emission region, m_e is the rest mass of an electron, $L'_{\text{inj},i}$ and $\gamma'_{\text{inj},i}$ denote the luminosity and the Lorentz factor of the injected electrons respectively, with the start and finish times denoted by $T'_{s,i}$ and $T'_{f,i}$, respectively. Here, $H(x; a, b)$ denotes the Heaviside function defined by $H = 1$ if $a \leq x \leq b$, and $H = 0$ everywhere else.

2.1 Electron Kinetic Equation

After the fresh electrons are injected into the blob, they gain energies through accelerations and lose energies through radiative processes, and they may also escape from the blob. The resulting electron energy distribution (EED) can be determined by solving a Fokker-Planck equation, which takes the form (e.g., Park & Petrosian 1995)

$$\frac{\partial N'_e}{\partial t'} = \frac{\partial^2}{\partial \gamma'^2} \left(\frac{1}{2} \frac{d\sigma'^2}{dt'} N'_e \right) - \frac{\partial}{\partial \gamma'} \left(\langle \frac{d\gamma'}{dt'} \rangle N'_e \right) - \frac{N'_e}{t'_{\text{esc}}} + \sum_{i=1}^m \dot{Q}'_{e,i}, \quad (2)$$

where the first coefficient $\frac{1}{2} \frac{d\sigma'^2}{dt'}$ acts to broaden the shape of the particle distribution, and the second coefficient $\langle \frac{d\gamma'}{dt'} \rangle$ represents the mean electron acceleration rate, and t'_{esc} is the escape timescale.

The term $\frac{1}{2} \frac{d\sigma'^2}{dt'}$ is represented by the diffusion coefficient, which is associated with stochastic particle-wave interactions. In magnetohydrodynamic (MHD) turbulence, particles can exchange energy with resonant plasma waves, and the associated diffusion coefficient in the energy space is given by

$$D_{\gamma} = D_0 \gamma'^q, \quad (3)$$

where q represents the spectral index of the turbulent wave spectrum, and $D_0 \propto \frac{v_A^2}{\lambda_{\text{max}}^{q-1}} \left(\frac{\delta B'}{B'} \right)^2$ is dominantly determined by the Alfvén speed (v_A) and the cutoff scale in the turbulence spectrum (λ_{max}), and the ratio of the turbulence energy density in the dominant wave mode relative to the energy density of the background field ($\delta B'^2/B'^2$) (e.g., Dermer, Miller & Li 1996; Stawarz & Petrosian 2008; O'Sullivan, Reville & Taylor 2009).

Since the properties of the turbulences are highly uncertain (see Teraki & Asano 2019; Demidem et al. 2020, and references therein). In this study, we use $q = 2$ to simulate hard sphere scattering between the MHD waves and the electrons. This leads the acceleration timescale independent of the energy of electrons. For resonant scattering by the Alfvén waves, the index $q = 2$ may be supported by the numerical simulations of freely decaying MHD turbulence (Christensson, Hindmarsh & Brandenburg 2001; Brandenburg, Kahnishvili & Tevzadze 2015). It should be pointed out that $q = 2$ may be consistent with the nonresonant acceleration (Lynn et al. 2014; Teraki & Asano 2019; Demidem et al. 2020)

The mean acceleration rate is written as

$$\langle \frac{d\gamma'}{dt'} \rangle = \dot{\gamma}'_{\text{sto}} + \dot{\gamma}'_{\text{sh}} + \dot{\gamma}'_{\text{rad}}, \quad (4)$$

where $\dot{\gamma}'_{\text{sto}}$, $\dot{\gamma}'_{\text{sh}}$ and $\dot{\gamma}'_{\text{rad}}$ denote the mean rate of change of the electron energy due to stochastic particle-wave interactions, shock acceleration and radiative cooling processes, respectively. The acceleration rate due to stochastic particle-wave interactions is given by (e.g., Dermer, Miller & Li 1996; Becker et al. 2006)

$$\dot{\gamma}'_{\text{sto}} = \frac{1}{\gamma'^2} \frac{d}{d\gamma'} \left(\gamma'^2 D_{\gamma} \right) = 4D_0 \gamma', \quad (5)$$

and the acceleration rate due to repeated interactions with shock waves is given by (Drury 1983; Schlickeiser 1984)

$$\dot{\gamma}'_{\text{sh}} = A_{\text{sh}} \gamma', \quad (6)$$

where $A_{\text{sh}} \propto \kappa u_{\text{sh}}^2 / K_{\parallel}$ is mainly related with the volume filling factor of shock waves (κ), the speed of shock waves moving through plasma (u_{sh}) and the spatial diffusion coefficient (K_{\parallel}).

To minimize the number of model parameters that are difficult to be constrained by the observed broadband SED, we treat

D_0 and A_{sh} as physical parameters, which control the acceleration efficiency. Since both the shock and stochastic acceleration rates are linearly dependent on energy. In our approach, A_{sh} is expressed as $A_{\text{sh}} = 4aD_0$, and therefore a describes the relative importance of shock acceleration compared with the stochastic acceleration process. When $a > 1$, shock acceleration dominates; otherwise, stochastic acceleration dominates. Then, the total acceleration timescale due to the incorporation of the shock and stochastic acceleration processes can be expressed as

$$t'_{\text{acc}} = \frac{\gamma'}{\dot{\gamma}'_{\text{sto}} + \dot{\gamma}'_{\text{sh}}} = \frac{1}{4D_0(1+a)}. \quad (7)$$

The diffusion rate parameter D_0 can be evaluated using t'_{acc} and a by inverting the above equation to obtain $D_0 = [4(1+a)t'_{\text{acc}}]^{-1}$, and therefore we obtain

$$\frac{1}{2} \frac{d\sigma'^2}{dt'} = \frac{\gamma'^2}{4(1+a)t'_{\text{acc}}}, \quad \dot{\gamma}'_{\text{sto}} = \frac{\gamma'}{(1+a)t'_{\text{acc}}}, \quad \dot{\gamma}'_{\text{sh}} = \frac{a\gamma'}{(1+a)t'_{\text{acc}}}. \quad (8)$$

The radiative cooling rate of the accelerated electrons due to synchrotron and SSC processes can be written as the sum $\dot{\gamma}'_{\text{rad}} = -(b_{\text{syn}} + b_{\text{SSC}})\gamma'^2$, and

$$b_{\text{syn}} = \frac{4c\sigma_{\text{T}}}{3m_e c^2} U'_{\text{B}}, \quad (9)$$

$$b_{\text{SSC}} = \frac{4c\sigma_{\text{T}}}{3m_e c^2} \int_0^{\infty} u'_{\text{syn}}(\epsilon') f_{kn}(\epsilon', \gamma') d\epsilon', \quad (10)$$

where c is the speed of light, σ_{T} is the Thomson cross-section, $U'_{\text{B}} \equiv B'^2/8\pi$ denotes the energy density of the magnetic field, $u'_{\text{syn}}(\epsilon')$ denotes the energy density of the synchrotron radiation field, and the function $f_{kn}(\epsilon', \gamma')$ denotes the integration of the Compton kernel (Jones 1968), fully taking into account Klein-Nishina (KN) effects for an isotropic seed photon field (e.g., Dermer & Menon 2009; Hu et al. 2020).

Using the relation between the energy-diffusion coefficient and the spatial diffusion coefficient, $D_{\gamma} K_{\parallel} = \gamma'^2 \beta_{\text{A}}^2 c^2/9$ (Schlickeiser 1984, 1985), the escape timescale can be evaluated as

$$t'_{\text{esc}} \simeq \frac{R'^2}{K_{\parallel}} = \frac{9t'_{\text{dyn}}{}^2}{4(1+a)t'_{\text{acc}}\beta_{\text{A}}^2}, \quad (11)$$

with $t'_{\text{dyn}} = R'/c$ and β_{A} denoting the dynamical timescale and the Alfvén velocity normalized to the speed of light, respectively

Due to the fact that the diffusive escape velocity of electrons can not exceed the speed of light in vacuum, i.e., $t'_{\text{esc}} > t'_{\text{dyn}}$, one naturally obtains the condition

$$\frac{t'_{\text{acc}}}{t'_{\text{esc}}} < \frac{t'_{\text{acc}}}{t'_{\text{dyn}}} < \frac{9}{4(1+a)\beta_{\text{A}}^2}. \quad (12)$$

The Fokker-Planck equation is numerically solved through an implicit Crank-Nicholson (CN) scheme, which has the advantage of being unconditionally stable. We use a time step $\Delta t' = 0.02t'_{\text{dyn}}$ ¹ and a 6000 point energy grid over the range $1 \leq \gamma' \leq 10^7$ in our code.

¹ To obtain a precise result at any given time, the time step should be far smaller than the characteristic acceleration and the dominant energy loss timescales of the electrons radiating at the peak of the observed SED. Using Eq. 14, we can find $t'_{\text{syn}} = t'_{\text{acc}} \simeq 0.2t'_{\text{dyn}}$ for the typical values of the parameters used in our model

2.2 Equilibrium electron spectrum for single injection

The EED could achieve an approximate equilibrium, representing a balance between the competing processes of acceleration, cooling losses, electron injection and escape. A useful quantity is the equilibrium Lorentz factor, γ'_{eq} , which is determined from a balance between acceleration and cooling losses. Because of the Klein-Nishina effect, synchrotron radiation dominates the cooling effect at $\sim \gamma'_{\text{eq}}$ even if we include the SSC cooling. Thus, we approximately have the equilibrium electron Lorentz factor

$$\gamma'_{\text{eq}} = [b_{\text{syn}} t'_{\text{acc}}]^{-1}. \quad (13)$$

Using the δ -function approximation for the observed synchrotron peak frequency, $\nu_{\text{pk}} = \nu_0 B' \delta_{\text{D}} \gamma'^2_{\text{pk}}$, and assuming that γ'_{eq} could be approximately equal to γ'_{pk} , we find that the ratio of the acceleration timescale to the dynamical timescale is given by

$$\begin{aligned} \frac{t'_{\text{acc}}}{t'_{\text{dyn}}} &= (t'_{\text{dyn}} b_{\text{syn}})^{-1} \left(\frac{\nu_{\text{pk}}}{\nu_0 B' \delta_{\text{D}}} \right)^{-1/2} \simeq 0.173(1+z)^{1/2} \\ &\times \left(\frac{B'}{0.1 \text{ G}} \right)^{-3/2} \left(\frac{\delta_{\text{D}}}{10} \right)^{-1/2} \left(\frac{t_{\text{var}}}{1 \text{ day}} \right)^{-1} \left(\frac{\nu_{\text{pk}}}{10^{18} \text{ Hz}} \right)^{-1/2} \end{aligned} \quad (14)$$

where $\nu_0 = 4m_e c^2/3hB_{\text{cr}}(1+z)$ with $B_{\text{cr}} \simeq 4.41 \times 10^{13} \text{ G}$ denoting the critical magnetic field strength.

The time required for establishing equilibrium is approximately evaluated through (Appendix A)

$$\frac{t'_{\text{eq}}}{t'_{\text{dyn}}} \simeq 2 \frac{t'_{\text{acc}}}{t'_{\text{dyn}}} \ln(\gamma'_{\text{eq}}/\gamma'_{\text{inj}}), \quad (15)$$

where γ'_{inj} is the Lorentz factor of injected electrons.

In the following, we present the approximate equilibrium distributions at t'_{eq} for the impulsive and continual injections of mono-energetic electrons. For the cooling process, we take into account the synchrotron energy loss alone. We inject a mono-energetic electron distribution with $\gamma'_{\text{inj}} = 10^2$.

2.2.1 Impulsive Injection

In the case of impulsive injection with inefficient escape, the electrons can reach the equilibrium between acceleration and energy losses. In the case, the electron injection luminosity, L'_{inj} , can be related with several observables, which is given by (Appendix B)

$$L'_{\text{inj}} \simeq \frac{4\pi d_L^2 F_{\text{syn}}}{(\nu_{\text{pk}}/\nu_0)} \frac{\gamma'_{\text{inj}} B'}{\Delta T'_{\text{inj}} b_{\text{syn}} \delta_{\text{D}}^3} \quad (16)$$

where $\Delta T'_{\text{inj}}$ is the duration of injection and F_{syn} denotes the total flux of the synchrotron bump².

In Fig. 1, we plot the equilibrium electron spectrum (solid lines in upper panel) and the corresponding synchrotron spectra produced by the three EEDs. Moreover, the temporal evolution of electron spectrum for $a = 10$ is shown in the upper panel of Fig. 1. In our simulations, we set $\Delta T'_{\text{inj}} = \Delta t'$ to mimic the instantaneous injection, and the other parameters are: $B' = 0.1 \text{ G}$, $\delta_{\text{D}} = 10$, $\beta_{\text{A}} = 0.1$, $t_{\text{var}} = 0.3 \text{ day}$, $\nu_{\text{pk}} = 10^{18} \text{ Hz}$ and $F_{\text{syn}} = 10^{-9} \text{ ergs/cm}^2/\text{s}$. For the given values of the parameters, we can obtain $\gamma'_{\text{eq}} \simeq 5.3 \times$

² F_{syn} should be a factor of a few larger than the synchrotron peak flux $F_{\text{syn}}^{\text{pk}}$ in the $\nu - \nu F_{\nu}$ space. The accurate relation between F_{syn} and $F_{\text{syn}}^{\text{pk}}$ depends on the detail shape of the equilibrium distribution.

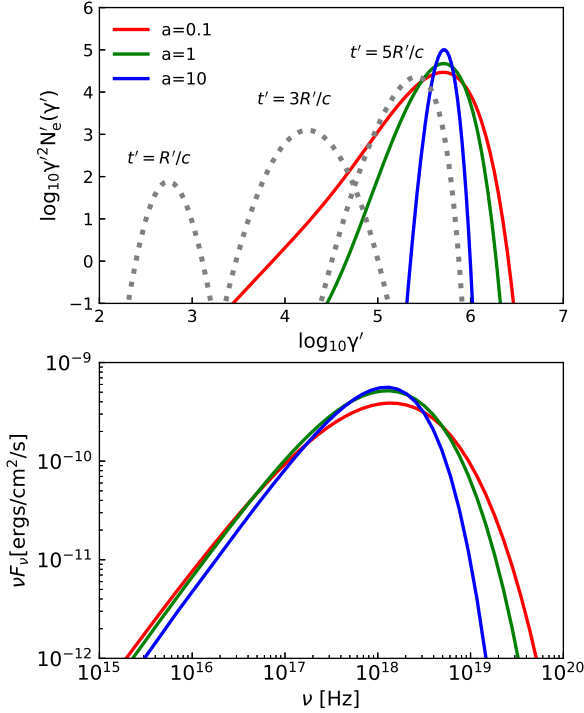


Figure 1. Equilibrium EEDs (solid lines in upper panel) and the corresponding synchrotron spectra produced by the three EEDs (lower panel) in the case of impulsive injection with inefficient escape. The evolution of EED for $a = 10$ is also showed (dotted lines in upper panel). The used model parameters can be found in context.

10^5 , $L'_{\text{inj}} \approx 1.5 \times 10^{39}$ ergs/s, $t'_{\text{acc}}/t'_{\text{dyn}} \approx 0.58$, $t'_{\text{eq}}/t'_{\text{dyn}} \approx 5$, and $t'_{\text{esc}}/t'_{\text{dyn}} \approx 350, 192, 35$ for $a = 0.1, 1, 10$, respectively.

It can be seen from Fig. 1 that the width of the equilibrium distribution increases with decreasing of a . When the shock acceleration is mainly responsible for the energy gain of electrons, e.g., $a = 10$, all the electrons will be accelerated to the equilibrium energy gradually, and a quasi-monoenergetic population of electrons is produced around the equilibrium energy. This is different from that produced in the case of the stochastic acceleration, where a quasi-Maxwellian distribution is formed (also see Katarzyński et al. 2006; Tramacere, Massaro & Taylor 2011). Note that the pileup distribution has been successfully employed to reproduce the hard spectra of γ -ray emission observed in several TeV blazars (Lefa et al. 2011; Asano et al. 2013).

It should be pointed out that the equilibrium distribution can be treated to be stationary as long as the equilibration timescale $t'_{\text{eq}} \ll t'_{\text{esc}}$. On the other hand, we stress that the choice of γ'_{inj} cannot affect the equilibrium electron spectrum.

2.2.2 Continuous injection

In the case of continuous injection, the competition between the acceleration and the escape can produce a power-law distribution when $\gamma' \ll \gamma'_{\text{eq}}$. The power-law index of the equilibrium distribution is given by (Appendix C)

$$n = \left(\frac{1}{2} + 2a \right) - \sqrt{\left(\frac{3}{2} + 2a \right)^2 + 4(1+a) \frac{t'_{\text{acc}}}{t'_{\text{esc}}}}. \quad (17)$$

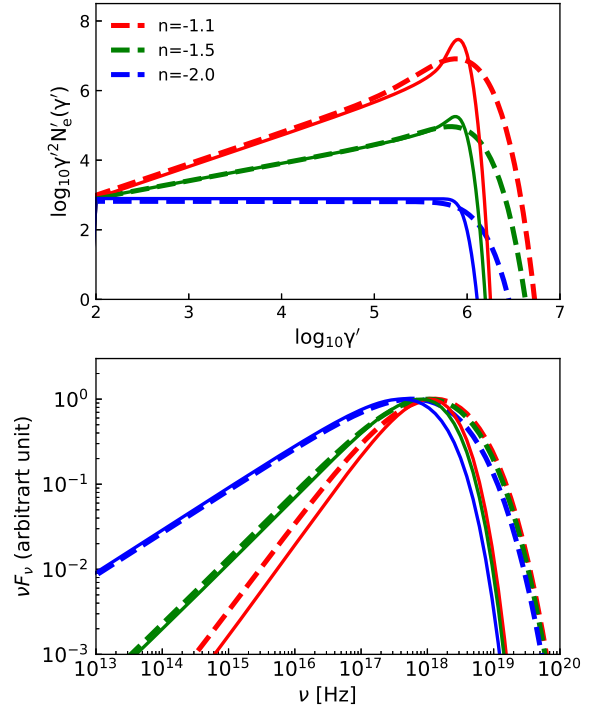


Figure 2. Equilibrium EEDs (upper panel) and the corresponding synchrotron spectra produced by the EEDs (lower panel) in the case of continuous injection. The thin solid and thick dashed lines represent $a = 10$ and $a = 0.1$, respectively.

Therefore, we can obtain

$$\frac{t'_{\text{acc}}}{t'_{\text{esc}}} = \frac{n^2 - (1+4a)n - (2+4a)}{4(1+a)}, \quad (18)$$

with a given value of a and n . Subsequently, we can calculate the Alfvén velocity by inverting Equation 11, which yields

$$\beta_A = \frac{3}{2\sqrt{1+a}} \left(\frac{t'_{\text{acc}}}{t'_{\text{esc}}} \right)^{1/2} \left(\frac{t'_{\text{acc}}}{t'_{\text{dyn}}} \right)^{-1}, \quad (19)$$

where $t'_{\text{acc}}/t'_{\text{dyn}}$ is derived through Equation 14. It is worth stressing that $t'_{\text{acc}}/t'_{\text{dyn}}$ and $t'_{\text{acc}}/t'_{\text{esc}}$ should satisfy the requirement of the Inequality 12.

In Fig. 2, we show the equilibrium EEDs (upper panel), together with the corresponding synchrotron spectra produced by the EEDs. For comparison, two values of $a = 0.1$ and $a = 10$ are adopted in the simulations, and the produced synchrotron spectra are normalized to their peak flux. To satisfy the requirement of Inequality 12, the magnetic field strength B' is assumed to be 0.04 G, while the values of t_{var} , ν_{pk} , δ_{D} are same as that in the impulsive injection. We use $L'_{\text{inj}} = 10^{39}$ ergs/s. With respect to the impulsive injection, we can use n as a model parameter which can be estimated by the spectral index of the observed synchrotron emission.

With the given values of the parameters, the characteristic acceleration and equilibrium times obtained in the tests are $t'_{\text{acc}}/t'_{\text{dyn}} \approx 2.32$ and $t'_{\text{eq}}/t'_{\text{dyn}} \approx 42$, respectively. When the stochastic acceleration dominates, i.e., $a = 0.1$, we obtain $(t'_{\text{acc}}/t'_{\text{esc}}, \beta_A) = (1.0, 0.62)$, $(0.44, 0.41)$ and $(0.08, 0.17)$, for $n = -2.0, -1.5$ and -1.1 respectively. When the shock acceleration dominates, i.e., $a = 10$, we obtain $(t'_{\text{acc}}/t'_{\text{esc}}, \beta_A) = (1.0, 0.19)$, $(0.49, 0.14)$ and

Table 1. Model parameters: the radius of the blob R' is determined by the causality relation (in unit of cm); the observed variability timescale t_{var} is in unit of day; the magnetic field strength B' is in unit of G; the Alfvén velocity β_A is in unit of the light speed; the diffusion coefficient D_0 is inferred by Eq. 7 (in unit of s^{-1}); the acceleration timescale t'_{acc} is determined by Eq. 14; the peak frequency $\nu_{\text{pk},1}$ is in unit of Hz; the total flux of the synchrotron bump $F_{\text{syn},1}$ is in unit of $\text{ergs}/\text{cm}^2/\text{s}$; the electron injection luminosity $L'_{\text{inj},1/2}$, in unit of ergs/s , is derived by Eq. 16; γ'_{eq} and $\gamma'_{\text{pk},2}$ are the electron Lorentz factor corresponding to $\nu_{\text{pk},1} = 5 \times 10^{18}$ Hz and $\nu_{\text{pk},2} = 5 \times 10^{16}$ Hz, respectively. The equilibrium timescale t'_{eq} and the escape timescale t'_{esc} are determined by Eq. 15 and Eq. 11, respectively. Note that all the timescales are in unit of the dynamical timescale t'_{dyn} .

Model	A	B	C	D
R'	2.01×10^{16}	2.01×10^{16}	2.51×10^{16}	3.01×10^{16}
t_{var}	1.0	1.0	1.0	1.0
β_A	0.03	0.03	0.03	0.03
a	7.0	7.0	3.0	3.0
B'	5.9×10^{-2}	5.9×10^{-2}	3.6×10^{-2}	2.0×10^{-2}
δ_D	8.0	8.0	10.0	12.0
D_0	2.4×10^{-7}	2.4×10^{-7}	2.05×10^{-7}	7.76×10^{-8}
t'_{acc}	0.19	0.19	0.36	0.8
$\nu_{\text{pk},1}$	5×10^{18}	5×10^{18}	5×10^{18}	5×10^{18}
$F_{\text{syn},1}$	3×10^{-9}	4.8×10^{-9}	3×10^{-9}	3×10^{-9}
t'_{eq}	3.08	3.08	5.89	13.32
t'_{esc}	1.6×10^3	1.6×10^3	1.7×10^3	7.8×10^2
γ'_{eq}	1.71×10^6	1.71×10^6	1.96×10^6	2.40×10^6
$\gamma'_{\text{pk},2}$	1.71×10^5	1.71×10^5	1.96×10^5	2.40×10^5
$\gamma'_{\text{inj},1}$	6×10^2	6×10^2	6×10^2	6×10^2
$L'_{\text{inj},1}$	6.58×10^{39}	1.37×10^{38}	4.43×10^{39}	3.86×10^{39}
$T'_{f,1}$	0.02	1.54	0.02	0.02
$\gamma'_{\text{inj},2}$	6×10^2	6×10^2	6×10^2	6×10^2
$L'_{\text{inj},2}$	11.5×10^{39}	10.88×10^{39}	6.5×10^{39}	2.47×10^{39}
$T'_{s,2}$	1.54	1.54	2.94	6.66
$T'_{f,2}$	2.74	2.74	5.10	11.52

(0.1, 0.06), for $n = -2.0, -1.5$ and -1.1 , respectively. These indicate that the stochastic acceleration needs more inefficient escape to provide the required slope of electron spectrum. It is consistent with the fact the shock acceleration is more efficient than the stochastic acceleration.

One can see that in the stochastic acceleration case, the electron distribution close to the equilibrium energy can be described by a power-law turning into a log-parabola (PLL) shape, which is consistent with previous studies (e.g., [Tramacere, Massaro & Taylor 2011](#); [Yan, Zeng & Zhang 2012](#)); while, a very sharp cut-off above the equilibrium energy is formed in the shock acceleration. Thus, the produced synchrotron spectrum above the peak frequency drops much more rapidly than that produced by the EEDs resulting from the stochastic acceleration.

3 APPLICATION TO MRK 501

In this section, we explain the formation of the narrow spectral feature observed at ~ 3 TeV. We adopt a two-injection scenario.

In our model, the size of the source (R'), the characteristic acceleration time (t'_{acc}) and the luminosity of the first injection electrons ($L'_{\text{inj},1}$) could be derived from the relationships in Section 2 with the observed variability timescale (t_{var}), the synchrotron peak

frequency ($\nu_{\text{pk},1}$), and the total flux of the synchrotron emission ($F_{\text{syn},1}$). Therefore, we can describe the emission with the model parameters: $B', \delta_D, a, \beta_A, t_{\text{var}}, \nu_{\text{pk},1}, F_{\text{syn},1}, \gamma'_{\text{inj},1}, T'_{s,1}, T'_{f,1}, \gamma'_{\text{inj},2}, L'_{\text{inj},2}, T'_{s,2}$ and $T'_{f,2}$.

The shortest variability found in the MWL data sample is on the order of one day ([Acciari et al. 2020](#)), we therefore use $t_{\text{var}} = 1$ day. Since we consider a very inefficient electron escape from the blob, we fix β_A to 0.03, which is compatible with the quasi-linear theory (e.g., [Becker et al. 2006](#)). We fix $\gamma'_{\text{inj},1} = \gamma'_{\text{inj},2} = 600$. The values of $\gamma'_{\text{inj},1}$ and $\gamma'_{\text{inj},2}$ have negligible effect on the SSC emission. We set $T'_{s,1} = 0$ and $T'_{f,1} = \Delta t' = 0.02R'/c$ for the impulsive injection. When the first injection electrons are accelerated to be close to half of the equilibrium energy, we start the second injection. In our test, we find that $T'_{s,2}$ is not sensitive in modeling the SED. The time interval between the two injections can be estimated by Equation A2. The remaining parameters are free.

Fig. 3 shows SSC modeling to the observed SED of Mrk 501 during 2014 July 19 (MJD 56857.98). The values of the parameters are given in Table 1 (Model A), in which we list all input parameters and the physical quantities associated with our model. As shown in the figure, our modeling can reproduce the observed SED well when we select the evolution time $t'_{\text{evo}} = T'_{f,2} = 2.74t'_{\text{dyn}}$. We note that the optical-UV flux produced by the theoretical model is lower than the observed data. However, it may be consistent with the variability behavior of MWL observations, which showed that the variability in the optical-UV bands is much lower than that in X-ray and TeV energies ([Acciari et al. 2020](#)). This indicates that the optical-UV emissions have another origin.

We separate contributions of the different segments of the electron spectrum IC scattering different segments of the synchrotron photons. The results indicate that the narrow TeV bump at ~ 3 TeV is the contribution from the pileup bump of electrons IC scattering synchrotron photons produced by the power-law branch of electrons. Moreover, the high flux observed by *Swift*-BAT above 10 keV is interpreted as the synchrotron emission of the pileup bump of electrons which is resulting from the first injection, while the X-rays below ~ 1 keV is dominated by the contribution of the power-law branch of electrons resulting from the second injection. The peak frequency of the synchrotron emission produced by the power-law branch is located at $\nu_{\text{pk},2} \approx 5 \times 10^{16}$ Hz. With the given values of B' and δ_D reported in Table 1, one can obtain $\gamma'_{\text{pk},2} \approx 1.7 \times 10^5$, which is in good agreement with that obtained in the slow cooling model proposed by [Acciari et al. \(2020\)](#). It should be noted that our results are obtained by using a self-consistent physical model. Moreover, it is interesting to note that the shock acceleration rather than the stochastic acceleration is required to be dominant, i.e., $a > 1$.

To illustrate the impact of duration of the first injection, we also display the result of the SED modeling with $T'_{f,1} = T'_{s,2}$ in Fig. 4 with the parameters values listed in Table 1 (Model B). We have not found a significant difference between Model A and Model B. The pileup structure in the EED can be formed in both continuous and impulsive injections.

4 DISCUSSION AND CONCLUSIONS

In this work, the emitting electron distribution is determined by numerically solving a Fokker-Planck equation that self-consistently incorporates both shock and stochastic acceleration processes, radiative losses, as well as synchrotron self-absorption and internal $\gamma\gamma$ absorption.

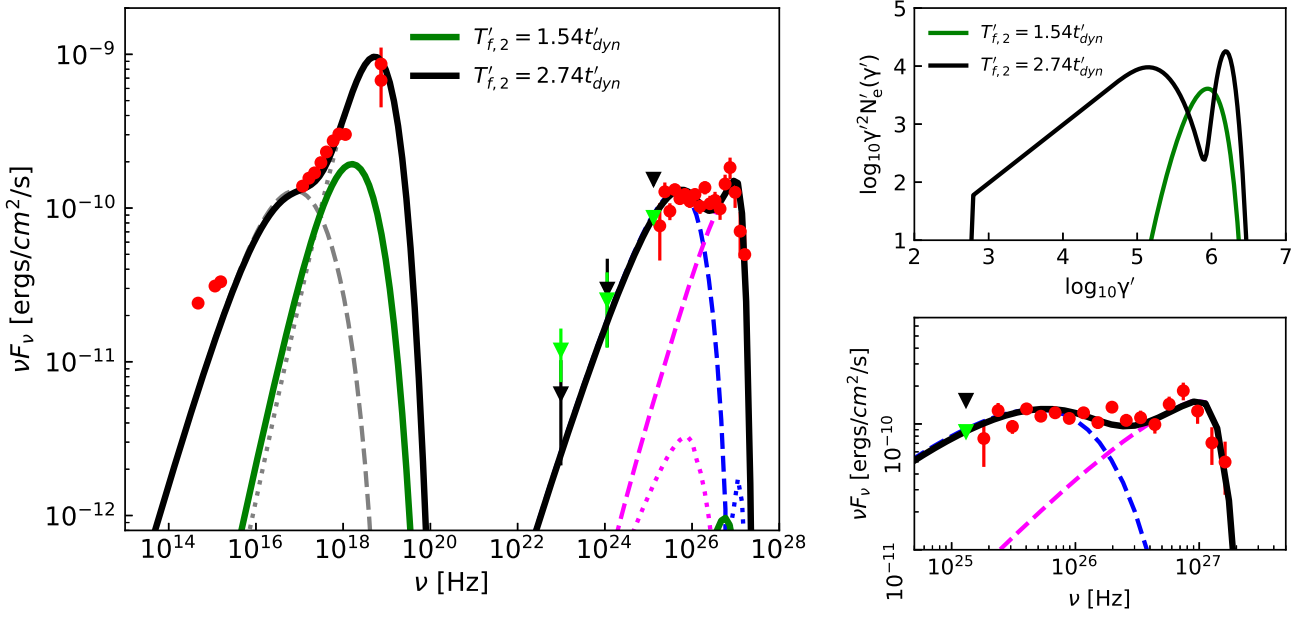


Figure 3. Modeling the broadband SED of Mrk 501 during 2014 July 19 (MJD 56857.98). The synchrotron-SSC emissions at $t'_{\text{evo}} = T'_{f,2} = 2.74t'_{\text{dyn}}$ (black solid line) and $t'_{\text{evo}} = T'_{f,2} = 1.54t'_{\text{dyn}}$ (olive line) are presented in the left panel. The EEDs at $t'_{\text{evo}} = T'_{f,2} = 2.74t'_{\text{dyn}}$ (black solid line) and $t'_{\text{evo}} = T'_{f,2} = 1.54t'_{\text{dyn}}$ (green line) are presented in the top right panel. In the left panel, we also present components in the SSC model at $t'_{\text{evo}} = T'_{f,2} = 2.74t'_{\text{dyn}}$. The gray dashed and dotted lines denote the synchrotron emission from the PL branch and pileup shape in the emitting EED, respectively. The corresponding SSC are denoted by the blue dashed and dotted lines, respectively. The magenta dotted line denotes the component that the synchrotron photons produced by the electrons of the PL branch are scattered by the electrons of the PL branch via IC scattering. The magenta dashed line denotes the component that the synchrotron photons produced by the electrons of the PL branch are scattered by the electrons of the pileup branch via IC scattering. The lower right panel shows the zoom-in view of the VHE SED. The *Fermi*-LAT data for 4 and 10 days time intervals are denoted by the black and green triangles, respectively. The MAGIC data from 0.1 TeV to 10 TeV have been corrected for EBL absorption according to the model of Domínguez et al. 2011. The X-ray data from *Swift*-XRT and *Swift*-BAT and VHE data can be safely considered simultaneous. Details about the data can be found in Acciari et al. 2020.

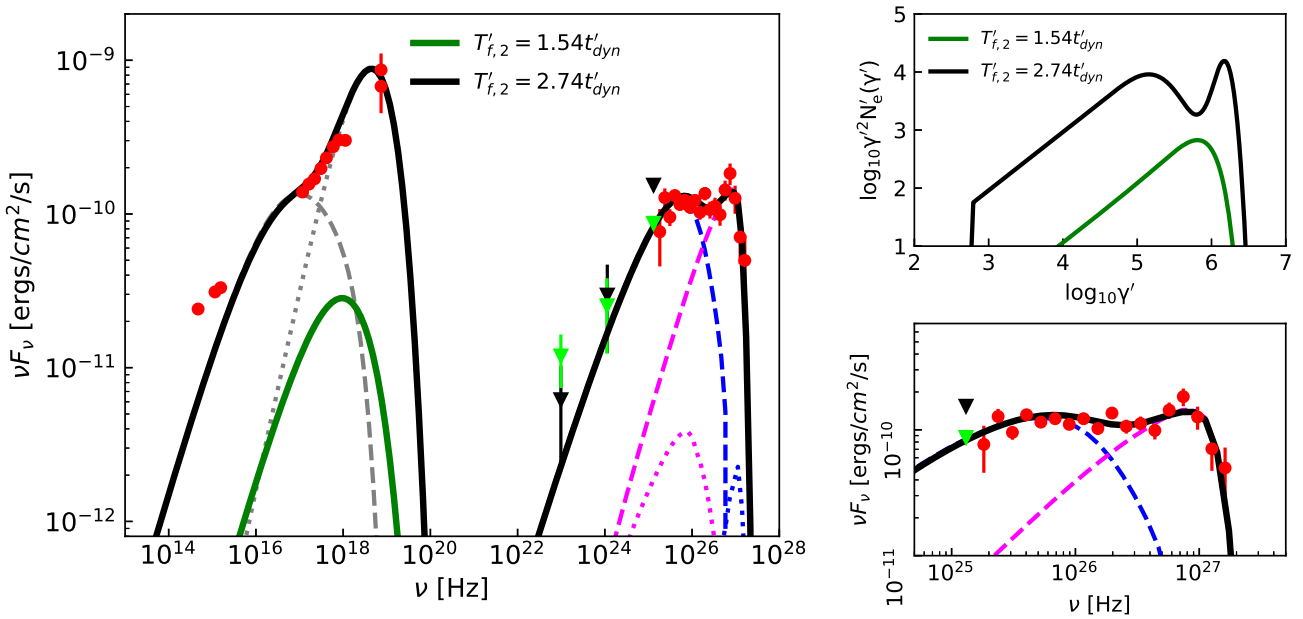


Figure 4. Same as Fig.3, except that the first population of electrons is continuously injected.

In the model, the parameters a , B' , δ_D and $T'_{f,2}$ are four key physical quantities to reproduce the observed SED. In the following, we examine the impact of the four parameters on SED modeling.

In Fig. 5, we show the modeling results with varying a . The narrow feature is not visible when the stochastic acceleration dominates over the shock acceleration, i.e., $a < 1$. The necessary condition for the formation of the pile-up in electron distribution is that the electrons are well confined within the emission zone (i.e., an inefficient electron escape). Additionally, two injection episodes of electrons are required to reproduce the SED of Mrk 501. Therefore, the narrow feature in the TeV energies disappears naturally if the electron escape effect will be important (i.e., efficient escape scenario), and/or the first population of electrons can be neglected (i.e., a single-injection scenario). In those cases, the broadband SEDs reported in Acciari et al. (2020) without the sharp TeV feature should be reproduced well following the prescription in Section 2.2.2.

A constraint on the Doppler factor δ_D can be obtained from transparency of γ -rays due to pair production absorption (e.g., Zdziarski & Lightman 1985; Finke, Dermer, & Böttcher 2008; Yan, Zeng, & Zhang 2012). Due to internal photon-photon annihilation, the optical depth for a γ -ray photon with observed energy E_γ can be estimated as (e.g., Abdo et al. 2011)

$$\tau_{\gamma\gamma} \approx \frac{\sigma_T E_\gamma F_0 (1+z)^2 D_L^2}{10 t_{\text{var}} m_e^2 c^6 \delta_D^6} \approx 4.65 \times 10^{-3} \quad (20)$$

$$\times \left(\frac{E_\gamma}{\text{TeV}} \right) \left(\frac{F_0}{10^{-11} \text{ erg/cm}^2/\text{s}} \right) \left(\frac{t_{\text{var}}}{\text{day}} \right)^{-1} \left(\frac{\delta_D}{10} \right)^{-6},$$

where F_0 is the observed monochromatic flux energy density at the observed photon energy

$$E_0 \approx \frac{2\delta_D^2 m_e^2 c^4}{E_\gamma (1+z)^2} \approx 50 \left(\frac{\delta_D}{10} \right)^2 \left(\frac{E_\gamma}{\text{TeV}} \right)^{-1} \text{ eV}. \quad (21)$$

Using $F_0 \approx 3 \times 10^{-11} \text{ erg/cm}^2/\text{s}$ at the observed energy $E_0 \approx 11.3 \text{ eV}$, one has $\tau_{\gamma\gamma}(3\text{TeV}) \approx 0.16$ for the given value of $\delta_D = 8$. This implies that δ_D used in Model A is close to the lower limit given by the transparency of γ rays.

Motivated by the above results, two typical values of $\delta_D = 10$ and 12 are used, and they are referred as Model C and Model D, respectively. In Fig. 6, we compare the modeling results of Models A, C and D. The parameters are given in Table 1. We find that the location of the narrow feature moves to higher energy for higher value of δ_D , and a decrease of B' and an increasing of $T'_{f,2}$ is required to reproduce the TeV spectrum below 3 TeV. Meanwhile, a smaller value of $a = 3.0$ is also needed for matching the observed X-ray spectrum and TeV spectrum below $\sim 3 \text{ TeV}$. It is worth noting that the duration of injection $\Delta T'_{\text{inj},2} = T'_{f,2} - T'_{s,2}$ can be predicted from the relation

$$\frac{\Delta T'_{\text{inj},2}}{t'_{\text{dyn}}} \approx \frac{t'_{\text{acc}}}{t'_{\text{dyn}}} \ln \frac{\gamma'_{\text{pk},2}}{\gamma'_{\text{inj},2}}, \quad (22)$$

where $\gamma'_{\text{pk},2} \approx \sqrt{\frac{\nu_{\text{pk},2}}{\nu_0 B' \delta_D}}$ is the peak frequency of the synchrotron component below 1 keV. Using $\nu_{\text{pk},2} = 5 \times 10^{16} \text{ Hz}$, we obtain that $\Delta T'_{\text{inj},2}/t'_{\text{dyn}}$ is 1.12, 2.14 and 4.89 for Model A, C and D, respectively. These values are in good agreement with that obtained from the SED modeling.

We find that the global properties of the jet including B' , δ_D and R' , as well as γ'_{eq} obtained in Model A are quite similar to that obtained by Acciari et al. (2020). Moreover, it can be seen from Table 1 that the value of the diffusion coefficient D_0

is $2.4 \times 10^{-7} \text{ s}^{-1}$. We find that similar result was obtained in other HBLs (e.g., Lewis, Becker & Finke 2016) and Fermi bubbles (Sasaki, Asano & Terasawa 2015).

In brief, we explain the broadband SED of Mrk 501 on 2014 July 19 by using a self-consistent one-zone leptonic jet model. In this model, the emitting EED is obtained by solving a Fokker-Planck equation including acceleration processes. Two injection episodes of electrons are needed to successfully explain the SED. The sharp and narrow spectral feature observed at $\sim 3 \text{ TeV}$ is resulting from the pileup branch of electrons IC scattering synchrotron photons produced by the PL branch of electrons. The extremely high flux observed by *Swift*-BAT above 10 keV is interpreted as the synchrotron emission from the pileup bump of electrons. The pileup branch of electrons is the accelerated first-injection-electrons, and the PL branch of electrons is the accelerated second-injection-electrons. Moreover, we find that shock acceleration is required to dominate over the stochastic acceleration in modeling the narrow peak feature in TeV spectrum. This is different from the stochastic scenario proposed by Acciari et al. (2020).

The scenario of multiple injections of relativistic electrons has been proposed to provide a explanation for the extreme flux variabilities of blazars (Röken & Schlickeiser 2009; Röken et al. 2018). Röken et al. (2018) argued that multiple-injection scenario is more realistic than single-injection scenario in blazar jets, as the blazar jets could extend over parsecs to tens of kiloparsecs scales, and thus likely pick up several electron populations from intergalactic media.

In principle, the narrow feature in the VHE spectrum of Mrk 501 is expected to be detected with high significance by CTA, which is designed to reach a sensitivity about an order of magnitude better than that of current imaging air Cherenkov telescopes and water Cherenkov telescopes (e.g., Actis et al. 2011; Acharya et al. 2013; Sol et al. 2013). The precise measurement of the TeV narrow feature by CTA could place strong constraints on the acceleration process working in the blazar jet.

ACKNOWLEDGEMENTS

We acknowledge the National Natural Science Foundation of China (NSFC-11803081, NSFC-12065011) and the joint foundation of Department of Science and Technology of Yunnan Province and Yunnan University [2018FY001(-003)]. The work of D. H. Yan is also supported by the CAS Youth Innovation Promotion Association and Basic research Program of Yunnan Province (202001AW070013).

DATA AVAILABILITY

No new data were generated or analysed in support of this research.

REFERENCES

- Abdo A. A. et al., 2010a, ApJ, 716, 30
- Abdo A. A. et al., 2010b, ApJ, 710, 1271
- Abdo A. A. et al., 2011, ApJ, 727, 129
- Acciari V. A. et al., 2020, A&A, 637, A86
- Acciari V. A. et al., 2021a, MNRAS, 504, 1427
- Acciari V. A. et al. 2021b, arXiv: 2106.05516
- Acharya B. S. et al., 2013, Astropart. Phys., 43, 3
- Actis M. et al., 2011, Exp. Astron., 32, 193

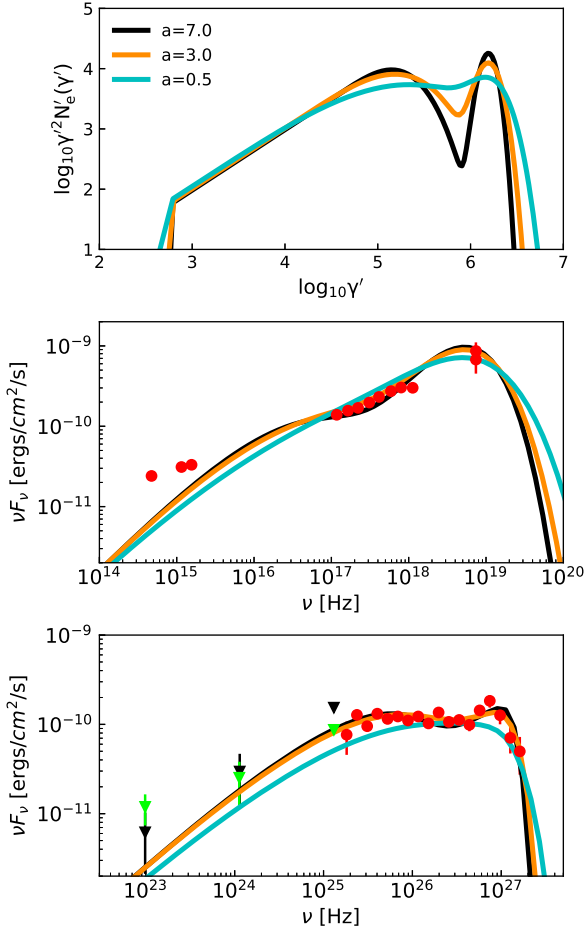


Figure 5. Theoretical SEDs produced by varying the parameter a . The top panel shows the EEDs. The remaining panels show the synchrotron (middle) and the SSC (bottom) spectra.

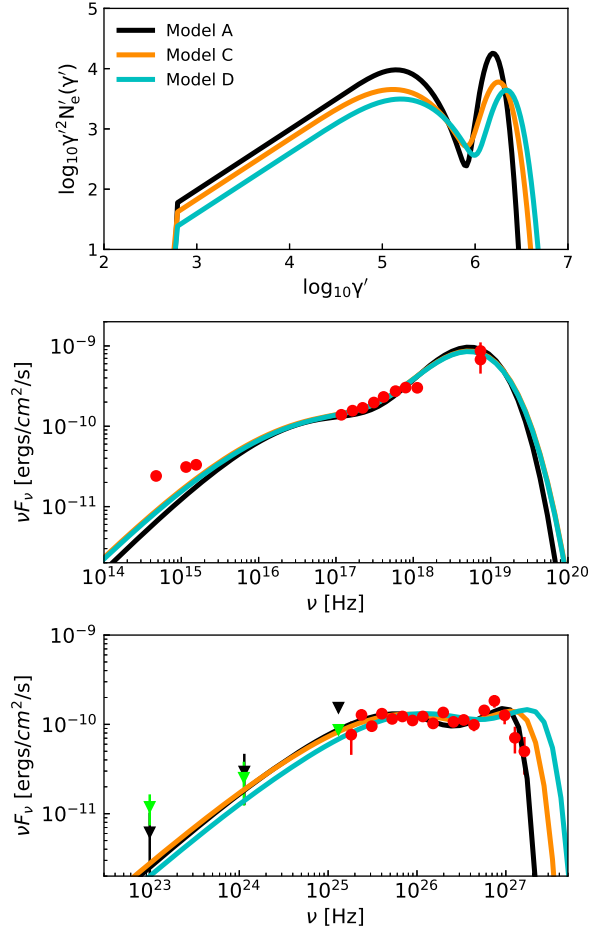


Figure 6. Theoretical SEDs of Models A, C, and D.

Ahnen M. L., Ansoldi S., Antonelli L. A. et al., 2018, *A&A*, 620, A181
 Aleksić J., Ansoldi S., Antonelli L. A. et al., 2015, *A&A*, 573, A50
 Asano K., Takahara F. et al., 2013, *ApJ*, 780, 64
 Bartoli B. et al., 2016, *ApJS*, 222, 6
 Becker P. A., Le T., Dermer C. D., 2006, *ApJ*, 647, 539B
 Brandenburg A., Kahniashvili T., Tevzadze A. G., 2015, *PhRvL*, 114, 075001
 Christensson M., Hindmarsh M., Brandenburg A., 2001, *PhRvE*, 64, 056405
 Demidem C., Lemoine M., Casse F., 2020, *PhRvD*.102b3003D
 Dermer C. D., Miller J. A., Li H., 1996, *ApJ*, 456, 106
 Dermer C. D., Menon G., 2009, *High Energy Radiation from Black Holes: Gamma Rays, Cosmic rays and Neutrinos*. Princeton Univ. Press, Princeton, NJ
 Dermer C. D., Cerruti M., Lott B. et al., 2014, *ApJ*, 782, 82
 Domínguez A., Primack J. R., Rosario D. J., et al., 2011, *MNRAS*, 410, 2556
 Drury L.O.C., 1983, *Rept. Progr. Phys.*, 46, 973
 Finke J. D., Dermer C. D., Böttcher M., 2008, *ApJ*, 686, 181
 Giommi P., Polenta G., Lähteenmäki A. et al., 2012, *A&A*, 541, A160
 Hayashida M., Madejski G. M., Nalewajko K. et al., 2012, *ApJ*, 754, 114
 Hu W., Yan D. H., Dai B. Z. et al., 2020, *MNRAS*, 493, 410
 Jones F. C., 1968, *Phys. Rev.*, 167, 1159
 Katarzyński K., Ghisellini G., Mastichiadis A., Tavecchio F., Maraschi L., 2006, *A&A*, 453, 47
 Kataoka J., Stawarz L., 2016, *ApJ*, 827, 55
 Katou T., Amano T., 2019, *ApJ*, 874, 119

Kirk J. G., Rieger F. M., Mastichiadis A., 1998, *A&A*, 333, 452
 Komissarov S. S., Vlahakis N., Königl A., Barkov M. V., 2009, *MNRAS*, 394, 1182
 Kroon J. J., Becker P. A., Finke J. D. et al., 2016, *ApJ*, 833, 157K
 Lefa E., Rieger F. M. et al., 2011, *ApJ*, 760, 64
 Lewis T. R., Becker P. A., Finke J. D., 2016, *ApJ*, 824, 108
 Lynn J. W., Quataert E., Chandran B. D. G., Parrish I. J., 2014, *ApJ*, 791, 71
 Maraschi L., Ghisellini G., Celotti A., 1992, *ApJL*, 397, L5
 Madejski G. M., et al., 2016, *ApJ*, 831, 142
 Nalewajko K., Begelman M. C., Sikora M., 2014, *ApJ*, 789, 161
 Narayan R., Kumar P., 2009, *MNRAS*, 394, L117
 Neronov A., Semikoz, D., Taylor A. M., 2012, *A&A*, 541, A31
 O’Sullivan S., Reville B., Taylor A. M., 2009, *MNRAS*, 400, 248
 Paliya V. S., Sahayanathan S., Stalin C. S., 2015, *ApJ*, 803, 15
 Park B. T., Petrosian V., 1995, *ApJ*, 446, 699
 Quinn J., Akerlof C. W., Biller S. et al., 1996, *ApJ*, 456, L83
 Röken C., Schlickeiser R., 2009, *ApJ*, 700, 460
 Röken C., Schuppan F., Proksch K., Schöneberg S., 2018, *A&A*, 616, A172
 Sasaki K., Asano K., Terasawa T., 2015, *ApJ*, 814, 93
 Schlickeiser R. 1984, *A&A*, 136, 227
 Schlickeiser R. 1985, *A&A*, 143, 431
 Shukla A., Chitnis V. R., Singh B. B. et al., 2015, *ApJ*, 798, 2
 Sol H. et al., 2013, *Astropart. Phys.*, 43, 215
 Stawarz L., Petrosian V., 2008, *ApJ*, 681, 1725
 Summerlin E. J., Baring M. G., 2012, *ApJ*, 745, 63
 Teraki Y., Asano K., 2019, *ApJ*, 877, 71T

- Tramacere A., Massaro E., Taylor A. M., 2011, ApJ, 739, 66
 Urry C. M., Padovani P., 1995, PASP, 107, 803
 Wendel C., Becerra González J., Paneque D., Mannheim K., 2021, A&A, 646, A115
 Yan D., Zeng H., Zhang L., 2012, PASJ, 64, 80
 Yan D. H., Zeng H. D., Zhang L., 2012, MNRAS, 424, 2173
 Yan D. H., Zeng H. D., Zhang L., 2014, MNRAS, 439, 2933
 Yan D. H., Yang S. B., Zhang P. F. et al., 2018, ApJ, 864, 164
 Zdziarski A. A., Lightman A. P., 1985, ApJ, 294, L79

APPENDIX A: EQUILIBRIUM TIMESCALE

Once the values of the acceleration timescale t'_{acc} and the equilibrium Lorentz factor γ'_{eq} have been obtained, we can compute the time needed for an electron with initial Lorentz factor γ'_0 to be accelerated to γ' , by integrating the mean acceleration rate without considering the SSC energy loss,

$$\frac{d\gamma'}{dt'} = -(\gamma'_{\text{eq}} t'_{\text{acc}})^{-1} \gamma'^2 + t'_{\text{acc}}^{-1} \gamma', \quad (\text{A1})$$

which yields

$$\Delta T'_d(\gamma'_0, \gamma') = t'_{\text{acc}} \ln \left(\frac{\gamma'_0 - \gamma'_{\text{eq}}}{\gamma'_0} \frac{\gamma'}{\gamma' - \gamma'_{\text{eq}}} \right), \quad (\text{A2})$$

for $\gamma'_0 \leq \gamma' < \gamma'_{\text{eq}}$. Indeed, the expression can be written in the form $\Delta T'_d(\gamma'_0, \gamma') \approx t'_{\text{acc}} \ln(\gamma'/\gamma'_0)$, when the acceleration dominates over the radiative cooling, i.e., $\gamma'_0 \leq \gamma' \ll \gamma'_{\text{eq}}$. Moreover, we have $\Delta T'_d(\gamma'_0, \gamma') = \gamma'_{\text{eq}}/2 \approx t'_{\text{acc}} \ln(\gamma'_{\text{eq}}/\gamma'_0)$.

Thus, the time t'_{eq} required for establishing equilibrium should be at least twice as much as $\Delta T'_d(\gamma'_0, \gamma'_{\text{eq}}/2)$. Here, we adopt a relatively conservative estimation $t'_{\text{eq}} = 2t'_{\text{acc}} \ln(\gamma'_{\text{eq}}/\gamma'_0)$.

APPENDIX B: INJECTION LUMINOSITY OF ELECTRONS WITH INEFFICIENT ESCAPE

The total luminosity of the synchrotron bump, neglecting self-absorption correction, can be expressed as (Dermer & Menon 2009)

$$\begin{aligned} L_{\text{syn}} &= m_e c^2 V' \delta_D^4 b_{\text{syn}} \int_1^\infty \gamma'^2 N'_e(\gamma') d\gamma' \\ &= m_e c^2 V' \delta_D^4 b_{\text{syn}} \langle \gamma'^2 \rangle N'_{\text{tot}}, \end{aligned} \quad (\text{B1})$$

where $\langle \gamma'^2 \rangle$ is the mean value of γ'^2 and N'_{tot} is the total number of electrons.

Since a quasi-Maxwellian distribution or a quasi-monoenergetic distribution could be expected to be formed after impulsive electron injection. We approximately have the relation

$$\langle \gamma'^2 \rangle \approx \gamma'^2_{\text{pk}} = \frac{\nu_{\text{pk}}}{\nu_0 B' \delta_D}, \quad (\text{B2})$$

where ν_{pk} is the peak frequency of the observed synchrotron bump.

In the case of a very inefficient electron escape, one has

$$N'_{\text{tot}} \approx \frac{L'_{\text{inj}} \Delta T'_{\text{inj}}}{V' \gamma'_{\text{inj}} m_e c^2} \quad (\text{B3})$$

based on the conservation of electron number.

Then, we can obtain an expression for L'_{inj} , by combining Equations B1, B2 and B3, which yields

$$L'_{\text{inj}} = \frac{L_{\text{syn}}}{\Delta T'_{\text{inj}} b_{\text{syn}} \delta_D^4 \gamma'^2_{\text{pk}}} \approx \frac{4\pi d^2 F_{\text{syn}}}{(\nu_{\text{pk}}/\nu_0)} \frac{\gamma'_{\text{inj}} B'}{\Delta T'_{\text{inj}} b_{\text{syn}} \delta_D^3} \quad (\text{B4})$$

where $\Delta T'_{\text{inj}}$ denotes the duration of injection and F_{syn} denotes the total flux of the synchrotron bump.

APPENDIX C: APPROXIMATE POWER-LAW SOLUTION

For the continual injection of monoenergetic electrons, the competition between the acceleration and the escape produces a power law distribution that extends from the injected Lorentz factor up to γ'_{eq} . Following the method presented in Kroon et al. (2016), we can obtain the power-law index of the resulting equilibrium distribution, which is in form of $N'_e(\gamma') = N_0 \gamma'^m$. By substituting the power-law form into Eq. 2, we can obtain a quadratic equation for n , given by

$$n^2 - (1 + 4a)n - [2 + 4a + 4\epsilon(1 + a)] = 0, \quad (\text{C1})$$

where $\epsilon = \frac{t'_{\text{acc}}}{t'_{\text{esc}}}$. The solution to this equation is

$$n_{\pm} = \frac{(1 + 4a) \pm \sqrt{(3 + 4a)^2 + 16\epsilon(1 + a)}}{2}. \quad (\text{C2})$$

Here, the positive power-law index n_+ applies below γ'_{inj} , and the negative index n_- applies for $\gamma'_{\text{inj}} \leq \gamma' \ll \gamma'_{\text{eq}}$. We find $n_- \approx (1/2) - \sqrt{9/4 + 4\epsilon}$ in the case of pure stochastic acceleration, i.e., $a \rightarrow 0$. In the case of pure shock acceleration, the power-law index n_- can be written as

$$n_- = \left(\frac{1}{2} + 2a \right) \left(1 - \sqrt{1 + \frac{2}{\frac{1}{2} + 2a} + \frac{3\epsilon + 1 + 2\epsilon(\frac{1}{2} + 2a)}{(\frac{1}{2} + 2a)^2}} \right). \quad (\text{C3})$$

Making a Taylor expansion in terms of the small quantity $y \equiv (\frac{1}{2} + 2a)^{-1}$, we obtain $n_- \approx -1 - \epsilon$. This is in agreement with previous work (Kirk, Rieger & Mastichiadis 1998).

This paper has been typeset from a $\text{\TeX}/\text{\LaTeX}$ file prepared by the author.